Kinematically complete study of electron transfer and rearrangement processes in slow Ar^{16+}-Ne collisions

Y. Xue,[1,2,*] R. Ginzel,[2] A. Krauß,[2] S. Bernitt,[2] M. Schöffler,[2,†] K. U. Kühnel,[2] J. R. Crespo López-Urrutia,[2] R. Moshammer,[2] X. Cai,[1] J. Ullrich,[2,3] and D. Fischer[2,‡]

[1]*Institute of Modern Physics, Chinese Academy of Sciences, Nanchang Rd. 509, 730000 Lanzhou, China*

[2]*Max-Planck-Institut für Kernphysik, Saupfercheckweg 1, D-69117 Heidelberg, Germany*

[3]*Physikalisch-Technische Bundesanstalt, Bundesallee 100, 38116 Braunschweig, Germany*

(Received 28 September 2014; published 24 November 2014)

The complete kinematics of single- and double-electron capture from neon to Ar^{16+} was measured with a reaction microscope at a projectile energy of 3.2 keV/u (velocity $v_p = 0.36$ a.u.). Not only the change of the electronic binding energies (the Q value) and the projectile scattering angles, but also (in the case of auto-ionization) the three-dimensional momentum vectors of the emitted electrons were determined. For single-electron capture, the Q-value spectrum shows strong population of both $n = 7$ and 8 states on the projectile, and weak contributions to $n = 6$ and 9 are also observed. In the case of double-electron capture, auto-ionizing double capture (ADC) dominates and the populations of $(n,n') = (5,7)$, $(6,6)$, $(6,7)$ and $(6,8)$ are observed, while true double capture (TDC) populates the $(5,7)$ state and asymmetric states of $(5,n')$ with $n' > 10$. The experimental cross sections for Auger decay with the electron energy E_e plotted as a function of the Q value suggest the occurrence of target excitation accompanying the population of configurations $(5,7)$ and $(6,6)$. No essential difference is found in the differential cross sections for ADC and TDC, and the angular distributions suggest that two-step processes dominate the double capture.

DOI: 10.1103/PhysRevA.90.052720 PACS number(s): 34.70.+e, 34.50.Fa

I. INTRODUCTION

In slow collisions of highly charged ions (HCIs) with neutral atoms, charge transfer from atoms to ions is the dominant process, which has intensively been studied in past decades (see, e.g., [1–5]). Besides its fundamental scientific significance, the charge transfer and the subsequent rearrangement dynamics of the excited many-electron systems formed are important for the characterization of plasmas, e.g., in nuclear fusion tokamaks or in astrophysical environments.

Today, single-electron capture (SEC) at low velocities ($v_p < 1$ a.u.) and for not-too-high projectile-charge states appears to be rather well understood. In general, an electron will be transferred at or near the crossings between the quasimolecular state corresponding to the incident channel and those correlated with the various nl levels. The captured electrons populate primarily only two or three excited projectile n shells (see, e.g., Refs. [6,7]), i.e., the process is highly state selective. Many aspects of this are well described by a multichannel Landau–Zener model (MCLZ) [2,8] or a classical over-barrier model (OBM) [3,9,10]. Much more accurate descriptions of SEC, even delivering differential cross sections (DCSs), are achieved with close-coupling (CC) calculations [11]. However, so far these methods are limited to ions with not-too-high charge states due to the considerable numerical effort connected to the increasing number of basis states that must be included. A special CC approach, the basis generator method (BGM) and its two-center extension (TC-BGM), describes charge transfer in slow ion-atom collisions and yields very good overall agreement with the experimental partial as well as DCSs [7]. So far, BGM calculations for highly charged projectile ions up to $q = 20$ are available.

In the case of double-electron capture (DEC), it is well-known that the capture of two electrons nearly always gives rise to doubly excited projectile states (n,n'), where n and n' are the principle quantum numbers. After the collision, the symmetric doubly excited projectile states $(n,n' \approx n)$ tend to decay rapidly via Auger electron emission, leaving a doubly charged target ion but a projectile retaining only one captured electron, known as auto-ionizing double capture (ADC). In contrast, asymmetric states, where the captured electrons have very different n, predominantly stabilize radiatively, leading to so-called true double capture (TDC). In general, symmetric states are often easy to populate through two sequential crossings with single-capture channels (see, e.g., Refs. [12–14]), while for asymmetric states, the population mechanisms have been intensively discussed. These include a one-step correlated double-capture process [15,16] where the entrance channel crosses the DEC channels and a two-step transfer involving electron-electron interaction referred to as correlated transfer excitation [12,14,16–18]. In addition, auto-transfer to Rydberg (ATR) [19–21] is also proposed. Via long-range coupling, it transfers a part of the population in symmetric states to the corresponding nearly degenerate Rydberg states on the way out of the collision.

In this paper, we use a reaction microscope [22] for a kinematically complete study of SEC and DEC in 3.2 keV/u Ar^{16+}-Ne collisions (projectile velocity of $v_p = 0.36$ a.u.). This technique allows 4π collection of the emitted electrons, maintaining at the same time the full resolution in the recoil-ion branch. Not only the Q values (electronic binding energies difference between the final and initial states) but also the projectile scattering angles of the capture processes are obtained. At the same time, in the case of the subsequent

*xueyl@impcas.ac.cn

†Present address: Institut fur Kernphysik, J. W. Goethe-Universität, Max-von-Laue-Strasse 1, 60438 Frankfurt am Main, Germany.

‡fischer@mpi-hd.mpg.de

auto-ionization, the three-dimensional (3D) momentum vectors of the emitted electrons are determined. The present results provide insights into the femtosecond dynamics of electron capture, as well as subsequent stabilization processes in charge-changing collisions between highly charged projectile ions and atoms.

II. EXPERIMENTAL SETUP

For the details of the reaction microscope and the setup of the beamline we refer to Ref. [6]. In brief, the HCIs were extracted from the Heidelberg electron-beam ion trap (HD-EBIT) and accelerated by a voltage of 8 kV. They were selected by their charge-to-mass ratio by a 90° dipole magnet and guided through a beamline to the reaction microscope. In the center of the microscope, the ion beam was intersected with a supersonically cooled Ne target jet. There, the recoiling target ions produced in collisions were extracted by a weak electric field (9 V/cm) along the projectile incoming beam direction. After being accelerated over a distance of 11 cm, the recoil ions passed a field-free region of 22 cm and were detected by a position-sensitive detector (PSD). In contrast to our previous experiments [6,7] with this setup, the recoil-ion PSD has been changed to a larger diameter (ø 80 mm) and there is a bore (ø 6 mm) in its center [23]. The PSD was placed in the center of the beam line, and its central bore allows the primary beam to enter the reaction microscope. Electrons emitted in the collision were extracted into the opposite direction and registered by a second PSD placed on the left side along the beam line. A homogeneous magnetic field of about 15 Gauss tilted by 8° with respect to the projectile-beam direction was applied to confine the electron transverse motion. Thus, all electrons with energies below 200 eV were impelled onto the detector in a cyclotron motion. The projectiles were charge-state analyzed by an electrostatic cylindrical-plate spectrometer and detected by another PSD after passing the reaction microscope. The recoil-ion and electron momentum vectors were calculated from their positions on the detector and their times of flight. SEC was identified by detecting the Ne^{+} and Ar^{15+} ions in coincidence, while ADC and TDC were distinguished as a coincidence between Ne^{2+} and Ar^{15+} and Ar^{14+} ions, respectively. The electrons from ADC events were measured in coincidence to the Ne^{2+} and Ar^{15+} ions.

For electron-capture processes, the longitudinal momentum transfer to the recoil ion, i.e., along the beam-propagation direction, yields direct information on the reaction Q value: $p_{r\parallel} = Q/v_p - n_c v_p/2$. Here, v_p is the projectile velocity and n_c is the number of electrons transferred. The transverse recoil-ion momentum, on the other hand, is related to the projectile scattering angle by $p_{r\perp} = m v_p \vartheta$ (for small scattering angles), with m being the projectile mass. Atomic units are used throughout the paper, unless otherwise indicated.

In the present experiment, a recoil-ion longitudinal momentum resolution of $\Delta_{r\parallel} = 0.3$ and 0.9 a.u. for SEC and DEC, respectively, was achieved, corresponding to a Q-value resolution of 3.0 and 8.8 eV. This relatively low resolution is due to the high electric field which was chosen to increase the electron-energy acceptance. The angular resolution is about 68 and 93 μrad for SEC and DEC, respectively. In the case of ADC, the electron longitudinal momentum resolution is about $\Delta p_{e\parallel} = 0.07$ a.u. Modulated by the cyclotron motion in the magnetic field, the electron transverse-momentum information is lost at certain times of flight (multiple integers of the inverse cyclotron frequency) [24]. The averaged transverse-momentum resolution is about $\Delta p_{e\perp} = 0.37$ a.u. The achieved average energy resolution is about $\Delta E_e = 10$ eV for the Auger electrons.

III. RESULTS

A. Single-electron capture

The present Q-value spectrum for SEC is shown in Fig. 1, where the numbers assigned to the peaks are the principal quantum numbers of the transferred electrons. The binding energies of the final projectile states were obtained by multiconfiguration Hartree–Fock (MCHF) calculations [25] and the deduced Q values, i.e., energy difference between the final projectile states and the initial target state (−21.6 eV), are shown as boxes in Fig. 1. The box width corresponds to the l splitting which is smaller for higher n where the electron states can be considered to be quasi-hydrogen-like.

Figure 1 shows that the electrons are predominately captured to $n = 7$ and $n = 8$ projectile states. The rather weakly populated channels of $n = 6$ and $n = 9$ are also observed. This result agrees with the expectations of OBM [3] (here, an effective main shell of $n_{\rm eff} = 7.8$ is obtained) or the MCLZ model. Compared with the results of Ar^{16+} interacting with helium at similar velocity [13], the dominant charge transfer takes place into even higher n shells of the projectile.

The present partial cross sections are shown in Fig. 2 and compared to the predictions of a MCLZ model [2] by using the semiempirical diabatic coupling elements of Olson and Salop [8]. The subshell-splitting modification factor [26] is neglected since the energy separations between the neighboring l levels are much smaller than the typical adiabatic energy splitting for the present case. In spite of the simplicity of the model

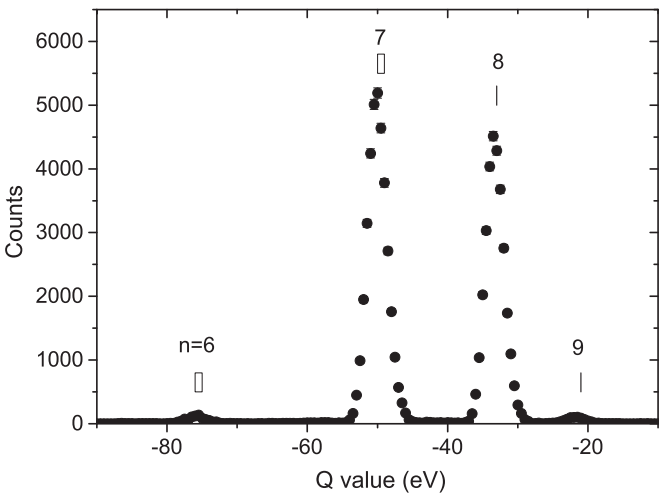

FIG. 1. Q-value spectrum for SEC in Ar^{16+}-Ne collisions at 3.2 keV/u. The top numbers represent the principal quantum number of the final projectile state $Ar^{15+}(n)$. The boxes indicate the Q values based on the MCHF calculation for the binding energies, with their widths related to the respective l-splitting.

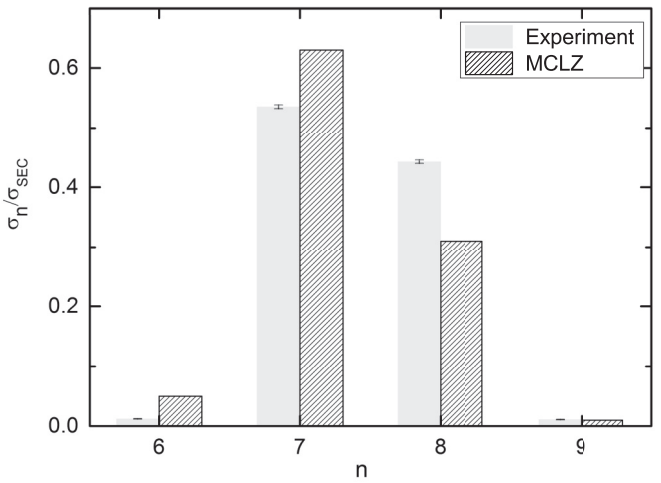

FIG. 2. Partial cross sections for the SEC channels in Ar^{16+}-Ne collisions at 3.2 keV/u, compared with the predictions of a MCLZ model.

neglecting rotational couplings [2], electron translation factors [2], and electron promotion [27,28], the calculation is in reasonable agreement with the experiment.

We present DCSs for SEC channels in Fig. 3. The average scattering angle shifts to larger values with decreasing n. The present results agree qualitatively with the model with respect to the fact that, according to the classical OBM or MCLZ models, capture to lower n requires smaller impact parameters than capture to higher n, resulting in larger scattering angles. In Fig. 3, the arrow denotes the location of the half Coulomb angle $\theta_C = Q/(2E)$ (E is the projectile energy), which is related to an impact parameter equal to the crossing radius in the curve-crossing picture if Coulomb potential curves are involved. As discussed in earlier studies (see, e.g., Refs. [13,29,30]), deflection to angles larger (smaller) than θ_C occurs for capture on the way in (out) along the semiclassical trajectory in curve-crossing space. The DCSs for capture into $n = 6$–9 states are about peaked at θ_C, which were also observed by Abdallah *et al.* [13,31] for Ar^{16+}- and Ar^{18+}-He collisions. These roughly equal cross sections lying inside and outside θ_C are due to the fact that the behavior at the crossing in the entrance channel is diabatic, which leads to nearly equal transfer probabilities on the way in and out. In order to quantitatively analyze the data, we carried out MCLZ calculations by using the method of Andersson *et al.* [32]. The calculations were convoluted with the angular resolution and normalized to approximately match the experimental peak heights. Obviously, this model poorly reproduces the shape of the observed spectra. Similar behavior was found in Ref. [13]. Although we have not made such a comparison here, Knoop *et al.* [7] showed that a TC-BGM calculation can give a good agreement with the experimental state-selective angular distribution.

B. Double-electron capture

In Fig. 4, we show the doubly DCSs for TDC and ADC as a function of the Q value and scattering angle. The calculated Q-value capture into (n,n') states, taken from Ref. [33], are

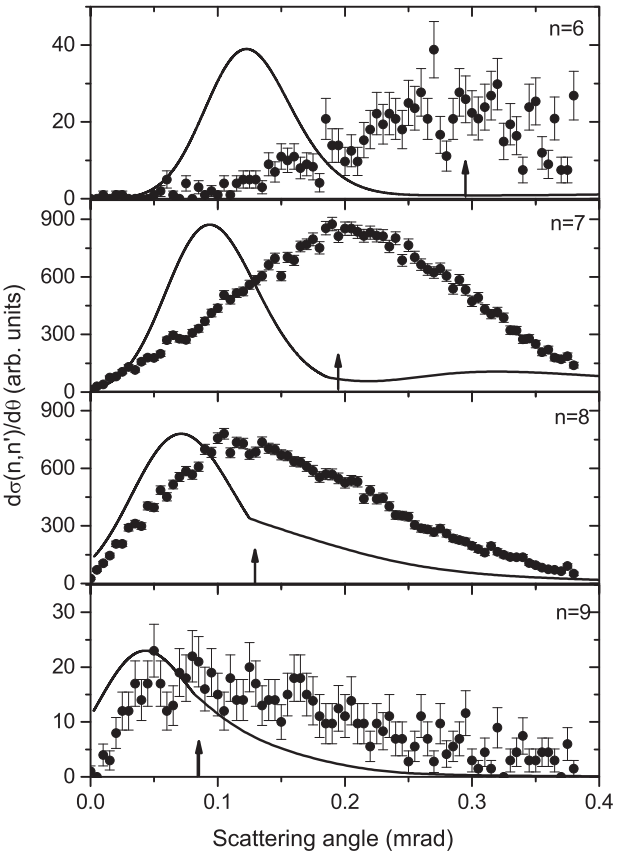

FIG. 3. Differential cross sections for SEC channels in Ar^{16+}-Ne collisions at 3.2 keV/u. The arrows show the locations of the half Coulomb angles. The solid lines represent the calculations of a MCLZ model by using the method of Andersson *et al.* [32]. They were folded with the present angular resolution and normalized to approximately match the experimental peak heights.

shown as boxes at the top of Fig. 4(a). The identifications of the observed (n,n') states are given at the bottom of each graph. $(n,n')^*$ and $(n,n')^{**}$ represent DEC associated with target excitation, which will be discussed later. In general, most of the doubly excited projectiles decay via Auger emission, leading to the overwhelmingly dominant ADC (about 92% contribution to DEC), while TDC contributes only with 8% to DEC. The events associated with a Q-value range of about -130 to -90 eV, corresponding to configurations (5,8) or (6,6), are much less prominent in the TDC spectrum. In contrast, an overwhelming majority of events in this range are observed in the ADC spectrum. We thus believe that most of those are related to the configuration (6,6), which is expected to have high Auger emission probability. In the TDC spectrum, although Q values for states of (6,7) and (6,8) overlap the asymmetric states of $(5,n')$, we believe that a majority of unresolved (n,n') states are asymmetric series $(5,n')$, which would be expected to have a larger radiative decay probability. Therefore, the populations of $(n,n') = (5,7)$, (6,6), (6,7), and (6,8) belong to ADC events, while TDC populates mainly configurations with $(n,n') = (5,7)$ and $(5,n')$ (with $n' > 10$).

In the case of ADC, the emitted electrons deliver additional information on the process and the subsequent Auger decay.

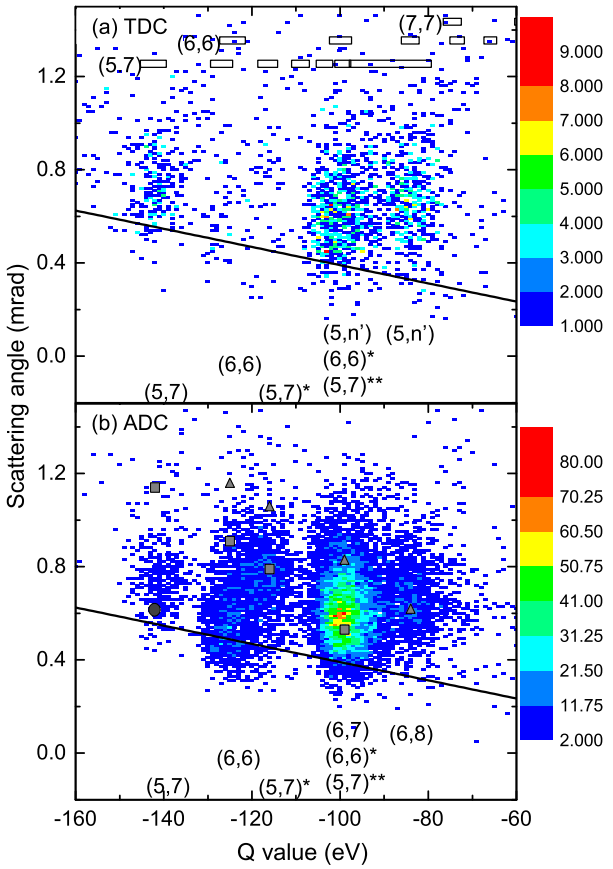

FIG. 4. (Color online) Doubly differential cross sections for (a) TDC and (b) ADC as a function of the Q value and scattering angle in Ar^{16+}-Ne collisions at 3.2 keV/u. The solid lines denote the locations of the half Coulomb angles. The three rows of boxes at the top indicate the expected Q-value ranges for the capture in the (n,n') states with $n = 7$ (top row), $n = 6$ (middle row), and $n = 5$ (bottom row) [33]. For each row, the left-most box corresponds to an n' as given by the number and it increments towards higher Q values. The observed (n,n') states are identified at the bottom of each graph. $(n,n')^*$ and $(n,n')^{**}$ represent DEC associated with target excitation. See the text for the small squares, triangles, and circle.

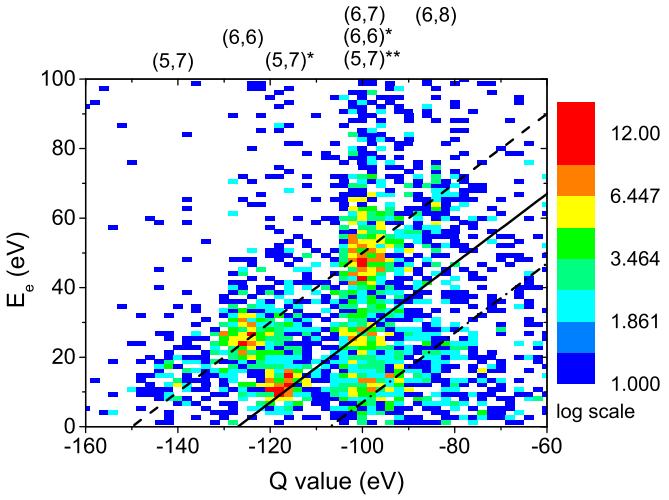

FIG. 5. (Color online) Differential cross section for ADC as a function of the Q value and electron kinetic energy in the projectile frame in Ar^{16+}-Ne collisions at 3.2 keV/u. The numbers in parentheses represent the main quantum numbers (n,n') of the two transferred electrons in the doubly excited projectile state, while $(n,n')^*$ and $(n,n')^{**}$ denote DEC associated with target excitation. See text for the lines.

The total electronic binding energy in the initial state is given by ε_i, and it changes by an amount, which is the Q value of the reaction, to the binding energy ε_m of the intermediate state due to the capture of two electrons. For ADC, the populated doubly excited projectile state decays after the collision, giving rise to the emission of an electron with kinetic energy E_e (in the projectile frame) and a final total electronic binding energy of ε_f. According to energy conservation,

$$E_e = \varepsilon_m - \varepsilon_f = Q + \varepsilon_i - \varepsilon_f. \quad (1)$$

In Fig. 5, we show the experimental DCSs for ADC as a function of the Q value and electron kinetic energy in the projectile frame. The dashed line shows the expected electron energies according to Eq. (1) for events where ε_f corresponds to projectile final configuration $Ar^{15+}(1s^2nl)$ with $n = 4$, i.e., the doubly excited state of Ar^{14+} decays and one of the active electrons finally populates the $n = 4$ state, while the other one is emitted with a kinetic energy that linearly depends on the Q values. Events with final projectile states $Ar^{15+}(1s^2nl)$ with $n = 3, n = 2$, or $n = 5$ are not observed because, for $n = 3$ and $n = 2$, the electron kinetic energy exceeds the spectrometer acceptance ($E_e < 200$ eV) and, for $n = 5$, the energy is not sufficient to promote an electron to the continuum.

Around the solid and the dash-dotted lines events are observed where the electron kinetic energies are about 23 and 43 eV smaller than expected. This can be explained by the simultaneous excitation of the remaining target ion [34], where one of the captured electrons was initially in the $2s$ shell or two loosely bounded electrons were captured but a third target electron initially in $2s$ ($2p$) was promoted to an excited target state with $nl = 2p$ ($3l$). For the data around the solid line, the corresponding processes are

$$\begin{aligned} &Ar^{16+}(1s^2) + Ne(1s^22s^22p^6) \\ &\quad \rightarrow Ar^{14+}(1s^2nn')^* + Ne^{2+}(1s^22s^12p^5) \\ &\quad \rightarrow Ar^{15+}(1s^24l) + Ne^{2+}(1s^22s^12p^5) + e. \end{aligned} \quad (2)$$

Here, $Ar^{14+}(1s^2nn')^*$ represents doubly excited projectile states with target excitation.

The Q values related to Eq. (2) are about -117 eV and -100 eV for $(n,n')^* = (5,7)^*$ and $(6,6)^*$, respectively (see Fig. 5); both shift about 23 eV with respect to those of the corresponding reactions

$$\begin{aligned} &Ar^{16+}(1s^2) + Ne(1s^22s^22p^6) \\ &\quad \rightarrow Ar^{14+}(1s^2nn') + Ne^{2+}(1s^22s^22p^4) \\ &\quad \rightarrow Ar^{15+}(1s^24l) + Ne^{2+}(1s^22s^22p^4) + e. \end{aligned} \quad (3)$$

These observations are in good agreement with the earlier-measured energy levels of Ne III [35], which resulted in binding-energy differences between $Ne^{2+}(1s^22s^12p^5)^3P$ and $Ne^{2+}(1s^22s^22p^4)^3P$, ^1D, ^1S of about 25, 22, and 18 eV,

respectively. The energy shift of about 43 eV observed for the events around the dash-dotted line can be explained by a final recoil-ion excitation state with the configuration of $Ne^{2+}(1s^2 2s^2 2p^3 3l)$.

It should be noted that there are alternative reaction channels that result in the same electron energies and Q values, e.g., if a photon is emitted from the doubly excited projectile ion before the projectile stabilizes via auto-ionization. For example, the process corresponding to events obtained for Eq. (2) with $(n,n')^* = (5,7)^*$ might be

$$\begin{aligned} &Ar^{16+}(1s^2) + Ne(1s^2 2s^2 2p^6) \\ &\quad \rightarrow Ar^{14+}(1s^2 5l 9l') + Ne^{2+}(1s^2 2s^2 2p^4) \\ &\quad \rightarrow Ar^{14+}(1s^2 5l 7l') + Ne^{2+}(1s^2 2s^2 2p^4) + h\nu \\ &\quad \rightarrow Ar^{15+}(1s^2 4l) + Ne^{2+}(1s^2 2s^2 2p^4) + h\nu + e. \quad (4) \end{aligned}$$

We do not believe that this process contributes significantly. On the one hand, we would expect to observe intensity related to (5,9) in the TDC spectrum, which however is not observed in Fig. 4. On the other hand, we would expect to observe radiative decay from (5,9) to (5,8), then the subsequent Auger decay with final projectile states of $Ar^{15+}(1s^2 4l)$ resulting in a higher electron energy (about 25 eV; see Fig. 5). Therefore, we believe that the events around the solid and the dashed-dot lines are mainly related to target excitation.

The present data also allow for a quantitative analysis of the importance of target excitations connected with the population of some projectile intermediate states and their decay modes. For the channel where the projectile decays from $Ar^{14+}(5,7)$ to $Ar^{15+}(4l)$, the recoiling target ion remains in an excited state after the collision with a probability of 91%, and this value amounts to 50% for the (6,6) state. In other words, the fraction of (5,7) and (6,6) population with simultaneous target excitation to the total ADC events related to final projectile states of $Ar^{15+}(1s^2 4l)$ are about 25% and 17%, respectively. We would like to mention that we cannot determine the fractions of target excitation for all DEC channels since, on the one hand, no electrons are ejected in TDC and, on the other hand, Auger electron energies associated with $Ar^{15+}(1s^2 3l)$ and $Ar^{15+}(1s^2 2l)$ exceed the spectrometer acceptance ($E_e < 200$ eV).

By projecting Fig. 4 onto the Q-value axis, we obtained the Q-value spectra for TDC and ADC and show them in Fig. 6. The numbers on the top represent the stabilization ratios $R(n,n')$ defined by

$$R(n,n') = \frac{\sigma_{\mathrm{TDC}}(n,n')}{\sigma_{\mathrm{TDC}}(n,n') + \sigma_{\mathrm{ADC}}(n,n')}, \quad (5)$$

where $\sigma_{\mathrm{ADC}}(n,n')$ and $\sigma_{\mathrm{TDC}}(n,n')$ are the ADC and TDC cross sections, respectively, for capture to a final configuration (n,n'). In the present work, the stabilization ratios were obtained by fitting Gaussian-peak shapes to the experimental Q-value spectra of TDC and ADC, and only these for pure (n,n') sets are shown.

It can be noted that the stabilization ratio for the configuration $(5,7)^*$ is only about 0.01, a factor of 25 lower than that for (5,7). At first sight this seems surprising because one might expect that the branching ratios of the projectile decay channels should be independent of the target ion left behind after the collision. However, there is an indirect dependence. The angular momentum of the doubly excited projectile intermediate state is strongly correlated to the final state of the target. The ratios of the decay modes of the projectile excited states, in turn, depend on the angular momentum including the sublevels, which are not resolved in our experiment (see, e.g., Ref. [16]). This leads to pronounced difference in stabilization ratios of (n,n') and $(n,n')^*$ observed in the experiment.

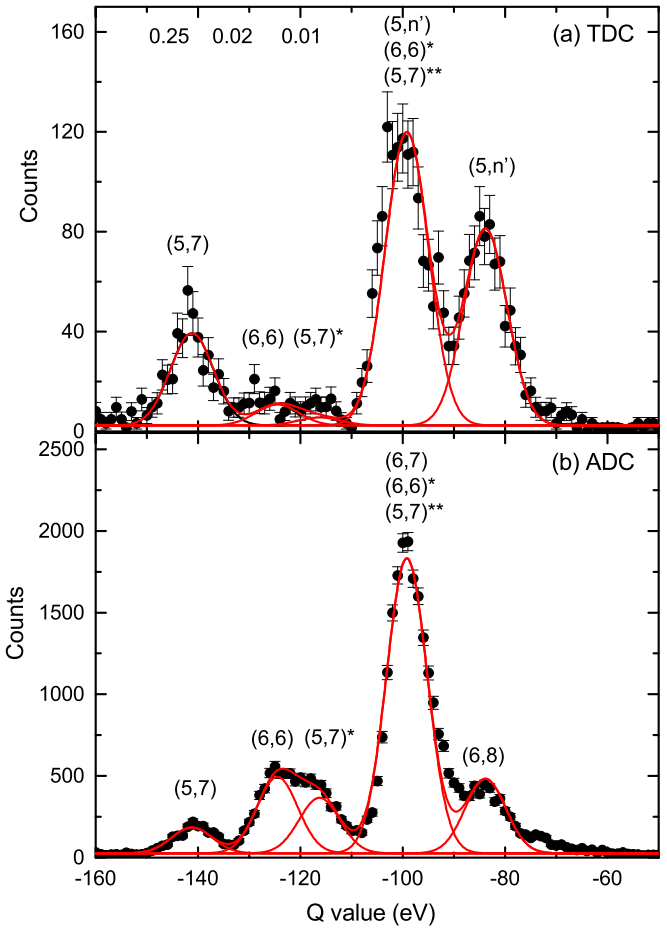

FIG. 6. (Color online) Experimental Q-value spectra for (a) TDC and (b) ADC in Ar^{16+}-Ne collisions at 3.2 keV/u. The numbers above represent the stabilization ratios. The solid curves show the Gauss fits for individual (n,n') shells. The numbers in parentheses represent the main quantum numbers (n,n') of the two transferred electrons in the doubly excited projectile state, while $(n,n')^*$ and $(n,n')^{**}$ denote DEC associated with target excitation.

The solid lines in Fig. 4 show the expected positions of the half Coulomb angle θ_C. For diabatic transitions, the maximum of the angular distribution is expected to be close to θ_C. Only the configuration of (6,6) shows a nearly θ_C-centered distribution, and thus it seems to be a one-step transition at the crossing between the DEC channel (6,6) and the incident channel. For the other configurations, the scattering angles strongly deviate from the observations in SEC, and the average deflection angles for DEC are substantially larger than θ_C. This phenomenon was also observed by Abdallah *et al.* [13] and Flechard *et al.* [12] and has been interpreted as being due to a population mechanism involving a two-step process rather

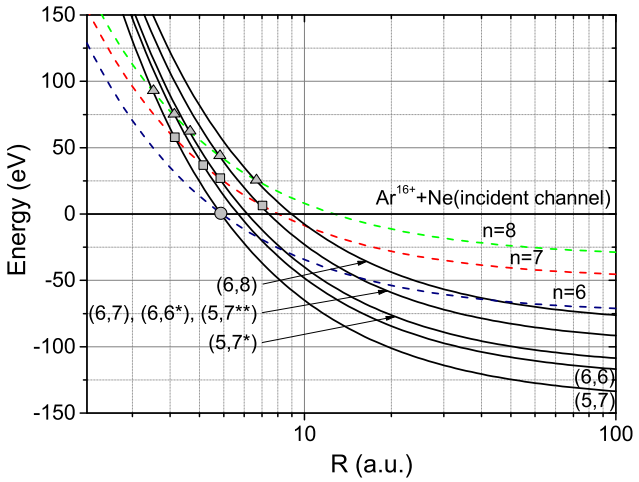

FIG. 7. (Color online) Coulomb potential curves for the system Ar^{16+}-Ne. Dashed and solid curves are related to single and double capture, respectively. The circle, squares, and triangles show two-step transitions via $n = 6$, 7, and 8, respectively.

than the direct transfer of two electrons at the crossing of the incident with the outgoing DEC channel.

In order to discuss the angular behavior of DEC, we employ the method proposed by Abdallah *et al.* [13] and estimate the scattering angle by using the classical trajectories and Coulomb potential curves (see Fig. 7), where for the incident channel the polarization interaction is neglected for simplicity. In Fig. 7, the circle, squares, and triangles show the two-step transitions via $n = 6$, 7, and 8 as the promoter potential curves, respectively. The corresponding calculated scattering

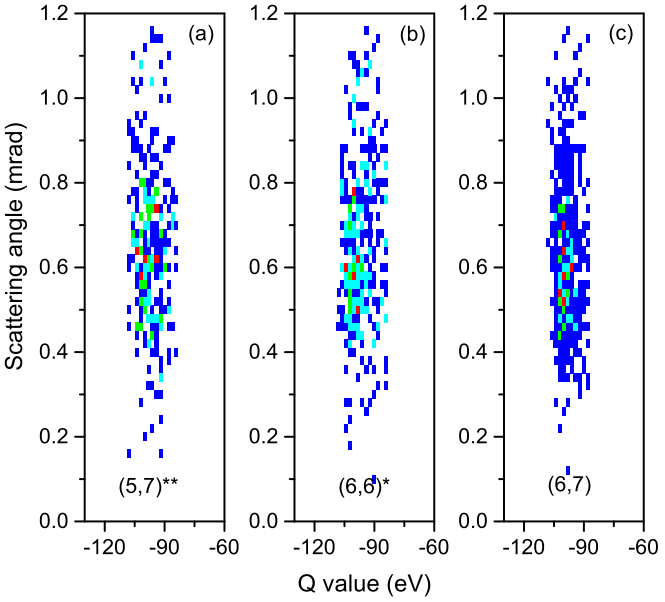

FIG. 8. (Color online) Doubly differential cross sections for the population of (a) $(5,7)^{**}$, (b) $(6,6)^{*}$, and (c) (6,7) as a function of the Q value and scattering angle in Ar^{16+}-Ne collisions at 3.2 keV/u. Events related to (a) $(5,7)^{**}$, (b) $(6,6)^{*}$, and (c) (6,7) were picked out in coincidence with an electron energy range (in projectile frame) of 0–19, 19–38, and 38–58 eV (see Fig. 5), respectively.

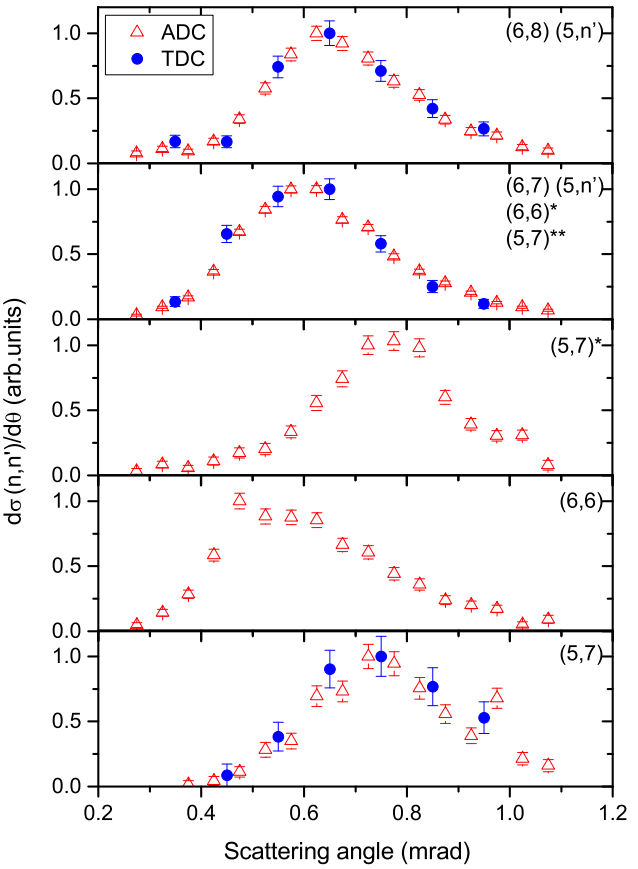

FIG. 9. (Color online) Differential cross sections for TDC (●) and ADC (△) in Ar^{16+}-Ne collisions at 3.2 keV/u. The experimental curves have been normalized independently to a peak height of unity. The numbers in parentheses represent the main quantum numbers (n,n') of the two transferred electrons in the doubly excited projectile state, while $(n,n')^{*}$ and $(n,n')^{**}$ denote DEC associated with target excitation.

angles are shown in Fig. 4 as circle, squares, and triangles, respectively. The comparison with experiment suggests that the $(5,7)^{*}$, (6,7), $(5,7)^{**}$, and $(6,6)^{*}$ states are populated in two steps via two successive one-electron captures involving the $n = 7$ single-capture channel. Here, first an electron is captured into the $Ar^{15+}(7l)$ state, which is the dominant SEC channel, and a second electron is captured at a smaller distance where this single-capture channel couples to various DEC curves, including those with target excitation. According to our simple model, the scattering angle for (6,7), $(5,7)^{**}$, and $(6,6)^{*}$ should be roughly the same. This we indeed observe by separating these three channels by selecting the corresponding Auger energies in ADC (see Fig. 8). The (5,7) state is populated in two steps via the $n = 6$ single-capture channel involving a transfer excitation mechanism in the second step, while the (6,8) state is fed via the $n = 8$ single-capture channel. In Fig. 9, we show the present DCSs for population of various series of doubly excited states. For the (6,6) and $(5,7)^{*}$ configurations, the DCSs for TDC are not shown due to the poor statistics. The data show that the DCSs for TDC and ADC are almost identical, suggesting similar trajectories for both cases in the curve-crossing picture. Thus, the asymmetric

states $(5,n')$ are also populated via two steps involving the $n = 7$ or $n = 8$ single-capture channel.

IV. CONCLUSIONS

We studied single- and double-electron capture in collisions of Ar^{16+}-Ne at 3.2 keV/u projectile energy with a reaction microscope. Q values and DCSs for SEC into $n = 6$–9 of $Ar^{15+}(n,l)$ and DEC into series of $(n,n') = (5,7), (5,n'), (6,6), (6,7)$, and $(6,8)$ were obtained. In the case of ADC, the 3D momentum vectors of the emitted electrons were determined in addition. For SEC, the Q-value spectrum shows strong population of both $n = 7$ and 8 states on the projectile, and weak contributions to $n = 6$ and 9 are also observed. For DEC, ADC dominates and target excitation accompanying DEC in configurations $(5,7)$, and $(6,6)$ is observed. The DCSs for ADC and TDC show no essential difference, and the angular distributions suggest that a two-step population mechanism dominates. Future experiments detecting the emitted photons and electrons at the same time could give insights into the subsequent stabilization processes in multi-electron-rearrangement collisions between highly charged projectile ions and atoms. A quantitative modeling of the obtained data seems to be involved and is presently not available.

ACKNOWLEDGMENTS

This work was supported by the Chinese Academy of Sciences (CAS) and the Max-Planck-Gesellschaft (MPG) through their joint doctoral promotion program and by the Alliance Program of the Helmholtz Association (HA216/EMMI).

[1] R. K. Janev and L. P. Presnyakov, Phys. Rep. **70**, 1 (1981).
[2] R. K. Janev and H. Winter, Phys. Rep. **117**, 265 (1985).
[3] A. Niehaus, J. Phys. B: At. Mol. Phys. **19**, 2925 (1986).
[4] M. Barat and P. Roncin, J. Phys. B: At., Mol. Opt. Phys. **25**, 2205 (1992).
[5] C. L. Cocke, in *Review of Fundamental Processes and Applications of Atoms and Ions*, edited by C. D. Lin (World Scientific, Singapore, 1993).
[6] D. Fischer, B. Feuerstein, R. D. DuBois, R. Moshammer, J. R. Crespo López-Urrutia, I. Draganic, H. Lörch, A. N. Perumal, and J. Ullrich, J. Phys. B: At., Mol. Opt. Phys. **35**, 1369 (2002).
[7] S. Knoop *et al.*, J. Phys. B: At., Mol. Opt. Phys. **41**, 195203 (2008).
[8] R. E. Olson and A. Salop, Phys. Rev. A **14**, 579 (1976).
[9] A. Bárány, G. Astner, H. Cederquist, H. Danared, S. Huldt, P. Hvelplund, A. Johnson, H. Knudsen, L. Liljeby, and K.-G. Rensfelt, Nucl. Instrum. Methods Phys. Res., Sect. B **9**, 397 (1985).
[10] L. Guillemot, P. Roncin, M. N. Gaboriaud, H. Laurent, and M. Barat, J. Phys. B: At., Mol. Opt. Phys. **23**, 4293 (1990).
[11] W. Fritsch and C. D. Lin, Phys. Rep. **202**, 1 (1991).
[12] X. Flechard, S. Duponchel, L. Adoui, A. Cassimi, P. Roncin, and D. Hennecart, J. Phys. B: At., Mol. Opt. Phys. **30**, 3697 (1997).
[13] M. A. Abdallah, W. Wolff, H. E. Wolf, E. Y. Kamber, M. Stöckli, and C. L. Cocke, Phys. Rev. A **58**, 2911 (1998).
[14] X. Fléchard, C. Harel, H. Jouin, B. Pons, L. Adoui, F. Frémont, A. Cassimi, and D. Hennecart, J. Phys. B: At., Mol. Opt. Phys. **34**, 2759 (2001).
[15] N. Stolterfoht, C. C. Havener, R. A. Phaneuf, J. K. Swenson, S. M. Shafroth, and F. W. Meyer, Phys. Rev. Lett. **57**, 74 (1986).
[16] N. Stolterfoht, K. Sommer, J. K. Swenson, C. C. Havener, and F. W. Meyer, Phys. Rev. A **42**, 5396 (1990).
[17] H. Winter, M. Mack, R. Hoekstra, A. Niehaus, and F. J. de Heer, Phys. Rev. Lett. **58**, 957 (1987).
[18] P. Roncin, M. Barat, M. N. Gaboriaud, L. Guillemot, and H. Laurent, J. Phys. B: At., Mol. Opt. Phys. **22**, 509 (1989).
[19] H. Bachau, P. Roncin, and C. Harel, J. Phys. B: At., Mol. Opt. Phys. **25**, L109 (1992).
[20] P. Roncin, M. N. Gaboriaud, M. Barat, A. Bordenave-Montesquieu, P. Moretto-Capelle, M. Benhenni, H. Bachau, and C. Harel, J. Phys. B: At., Mol. Opt. Phys. **26**, 4181 (1993).
[21] I. Sanchez and H. Bachau, J. Phys. B: At., Mol. Opt. Phys. **28**, 795 (1995).
[22] J. Ullrich, R. Moshammer, A. Dorn, R. Dörner, L. P. H. Schmidt, and H. Schmidt-Böcking, Rep. Prog. Phys. **66**, 1463 (2003).
[23] A. Krauß, Diplomarbeit Ruprecht-Karls-Universität Heidelberg, 2008 (unpublished).
[24] R. Moshammer, M. Unverzagt, W. Schmitt, J. Ullrich, and H. Schmidt-Böcking, Nucl. Instrum. Methods Phys. Res., Sect. B **108**, 425 (1996).
[25] C. Froese Fischer, *Computational Atomic Structure: An MCHF Approach* (Inst. Phys., Bristol, 2000).
[26] K. Taulbjerg, J. Phys. B: At. Mol. Phys. **19**, L367 (1986).
[27] M. Barat and W. Lichten, Phys. Rev. A **6**, 211 (1972).
[28] P. Roncin, M. N. Gaboriaud, L. Guillemot, H. Laurent, S. Ohtani, and M. Barat, J. Phys. B: At., Mol. Opt. Phys. **23**, 1215 (1990).
[29] L. N. Tunnell, C. L. Cocke, J. P. Giese, E. Y. Kamber, S. L. Varghese, and W. Waggoner, Phys. Rev. A **35**, 3299 (1987).
[30] L. Andersson, H. Danared, and A. Brny, Nucl. Instrum. Methods Phys. Res., Sect. B **23**, 54 (1987).
[31] A. Cassimi, S. Duponchel, X. Flechard, P. Jardin, P. Sortais, D. Hennecart, and R. E. Olson, Phys. Rev. Lett. **76**, 3679 (1996).
[32] L. R. Andersson, J. O. P. Pedersen, A. Barany, J. P. Bangsgaard, and P. Hvelplund, J. Phys. B: At., Mol. Opt. Phys. **22**, 1603 (1989).
[33] H. Cederquist, C. Biedermann, N. Selberg, and P. Hvelplund, Phys. Rev. A **51**, 2169 (1995).
[34] A. A. Hasan, E. D. Emmons, G. Hinojosa, and R. Ali, Phys. Rev. Lett. **83**, 4522 (1999).
[35] A. E. Kramida and G. Nave, Eur. Phys. J. D **37**, 1 (2006).